Predicting the Phase Behavior of ABAC Tetrablock Terpolymers: Sensitivity to Flory–Huggins Interaction Parameters

Akash Arora[a], Naveen Pillai[a,b], Frank S. Bates[a], Kevin D. Dorfman[a,c]

[a]*Department of Chemical Engineering and Materials Science, University of Minnesota–Twin Cities, 421 Washington Ave SE, Minneapolis, MN 55455, USA*
[b]*Present address: Department of Nuclear Engineering, North Carolina State University, Campus Box 7909, Raleigh, NC 27695, USA*
[c]*Email: dorfman@umn.edu*

Abstract

Self-consistent field theory (SCFT) is a powerful tool for discovering new nanostructures in self-assembling block polymers. However, the reliability of the resulting predictions depend strongly on the Flory-Huggins interaction parameters χ_{ij} used to quantify the excess free energy of mixing of different blocks i and j arising from segment-segment interactions. The problem is especially significant for multiblock polymers, owing to the multitude of χ_{ij} parameters and the sensitivity of the resulting phase behavior when the χ_{ij} do not differ substantially for different block pairs. To illuminate this issue, we examine how the SCFT-predicted phase behavior of a poly(styrene)-*b*-poly(isoprene)-*b*-poly(styrene)′-*b*-poly(ethylene oxide) (SIS′O) tetrablock terpolymer changes depending on the method used to estimate the trio of χ_{ij} parameters for this chemistry. SIS′O is an ideal model system for our purposes, as it exhibits a large number of poly(ethylene oxide) sphere-forming phases, emerging from the segregation of the poly(ethylene oxide) block due to the relatively high values of χ_{SO} and χ_{IO}, accompanied by subtle matrix segregation effects arising due to the smaller χ_{IS} between poly(isoprene) and poly(styrene). We first use χ_{IS},χ_{IO}, and χ_{SO} available in literature estimated using mean-field theory order–disorder transitions of the relevant diblock polymers. As this method is expected to lead to significant errors in χ_{ij} that propagate into the SCFT predictions, we also consider two fluctuation-corrected approaches to extract χ_{ij} from diblock polymer data, namely (i) fitting the order-disorder

transition temperature to that predicted by molecular dynamics simulations and (ii) renormalized one-loop theory predictions for the structure factor of the disordered state. While even the fluctuation-corrected χ parameters do not lead to SCFT phase behavior that exactly matches experiments, the SCFT calculations using the molecular dynamics-fitted χ parameters correctly predict stable Frank–Kasper A15 and σ phases. The results presented here highlight the challenges in predictively modeling the phase behavior of multiblock polymers using SCFT, a critical task for the discovery of new multiblock polymer materials.

Keywords: block polymer, Flory-Huggins theory, self-consistent field theory, phase behavior

---

1. Introduction

Block polymers self-assemble at nanometer length scales to form a wide variety of periodically ordered structures. Professor Takeji Hashimoto, to whom this article is dedicated in celebration of his extraordinary career in polymer science, contributed a wealth of foundational knowledge regarding the structure and properties of this class of soft materials. Even the simplest block polymers, the AB diblocks, form at least eight different morphologies [1, 2, 3, 4]. Multiblock polymers, comprising three or more blocks, offer a platform for creating a much larger array of ordered structures [5]. For example, linear ABC triblock terpolymers already have more than 30 known ordered phases [6, 7, 8, 9, 10, 11, 12, 13]. Varying the architecture from linear ABC to star ABC provides access to many more intriguing morphologies including quasicrystals [14, 15, 16, 17]. The freedom to select different block chemistries, and independently vary block lengths, further adds to the extraordinary design opportunities provided by this class of macromolecules [5].

Clearly, synthesizing a massive library of multiblock polymers with varying block compositions, chemistries, and architectures in the hope of discovering new ordered structures is inefficient and expensive. Hence, the discovery of new materials within such a vast molecular design space needs to be steered using theory and computation. Among various methods available, self-consistent field theory (SCFT) represents an efficient approach for exploring large parameter spaces [18, 19, 20, 21, 22]. However, the success of an SCFT-driven materials design program relies heavily

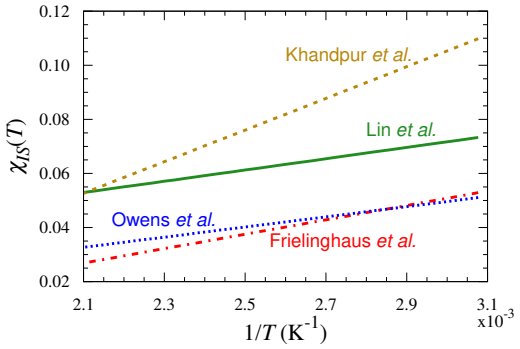

Figure 1: Comparison of Flory–Huggins interaction parameter χ_{IS} for poly(isoprene) and poly(styrene) reported by different publications [27, 28, 29, 30]. These parameters are obtained by performing experiments on PI-PS diblock copolymers. Here we note that it is important to use a common repeat unit volume when making such a comparison, and so all the above parameters are transferred to a chosen reference volume, $v_{\text{ref}} = 118$ Å^3.

on the input parameters used to perform the calculations. In particular, the Flory–Huggins parameter χ_{ij} describing the net interaction between two chemically distinct monomeric segments i and j is of paramount importance [23]. These parameters are typically obtained from the phase behavior of the corresponding diblock polymer, although simulation-based methods for predicting χ continue to advance [24, 25, 26]. As illustrated in Fig. 1 for the poly(isoprene)-*b*-poly(styrene) (IS) diblock copolymer, one of the most studied diblock systems, different data sets produce markedly different estimates for χ_{IS}, which then presumably translate into different SCFT predictions for the phase behavior of multiblock polymers containing poly(isoprene) and poly(styrene) as two of their blocks.

A key open question is determining the magnitude of the anticipated sensitivity of SCFT-predicted phase behavior to the input χ parameters for multiblock polymers. In this work, we address this question by considering a poly(styrene)-*b*-poly(isoprene)-*b*-poly(styrene)′-*b*-poly(ethylene oxide) (SIS′O) tetrablock terpolymer. Our choice is motivated by a host of recent experimental studies on SIS′O tetrablocks reporting an array of ordered structures including core-shell spheres and cylinders, the Frank–Kasper σ and A15 phases, and a dodecagonal quasicrystalline morphology [2, 31, 32, 33, 34]. We examine how the resulting SCFT phase diagrams are affected by the method used to estimate the χ parameters, focusing on the three standard approaches appearing in the literature. In the first

approach, we use the parameters reported in literature by Frielinghaus *et al.* [30, 35, 36], which were obtained by fitting the experimentally measured order–disorder transition temperatures (T_{ODT}) for volumetrically symmetric diblock copolymers ($f_{\mathrm{A}} = 0.5$) to the mean-field theory prediction of $\chi N_{ODT} = 10.5$ [37]. In the second approach, we searched the literature to find values of T_{ODT} for symmetric samples for each of the three diblocks, and fit those values to the χN_{ODT} predicted by coarse-grained molecular simulations [38, 39]. In the final approach, we use the interaction parameters reported in the PhD thesis of Pavani Medapuram [40], which were obtained by fitting the experimentally measured small-angle X-ray and neutron scattering (SAXS and SANS) intensities of the disordered phase to the predictions of the renormalized one-loop theory for symmetric diblock copolymers [41].

Our goal here is not to address *per se* the accuracy of a given method for predicting χ; this important problem would be best addressed by comparing theory to experiments using diblock polymers [42, 43]. Rather, our goal is to understand how the SCFT predictions for a model ABAC multiblock polymer differ depending on the method used to estimate χ. In this light, SIS'O is an ideal model system; there are experimental data to use as a point of reference [34], the system exhibits a large number of different phases over a rather narrow range in composition and temperature, and the different sphere-forming phases are very close in free energy. SIS'O thus should exhibit the exquisite sensitivity to the χ parameters that we anticipate will be a prevalent phenomenon in multiblock polymers, and could stymie attempts to model such materials. Inasmuch as the trio of approaches we use here to estimate χ are the standard starting points for any materials discovery program predicated on SCFT, the extreme sensitivity of the resulting phase behavior to the choice of χ parameters constitutes a cautionary tale for future SCFT-based designs of multiblock polymer materials.

2. Estimation of Flory–Huggins Interaction Parameters

2.1. Approach 1: χ from Mean-Field Theory

Frielinghaus *et al*. [30, 35, 36] reported the three binary interaction parameters required in this work. By fitting the order–disorder transition to

the predictions of mean-field theory, they obtained

$$\chi_{\mathrm{IS}} = \frac{26.63}{T} - 0.0290, \tag{1}$$

$$\chi_{\mathrm{SO}} = \frac{30.05}{T} - 0.0231, \tag{2}$$

$$\chi_{\mathrm{IO}} = \frac{91.48}{T} - 0.0584. \tag{3}$$

The above interaction parameters use a reference volume, $v_{\mathrm{ref}} = 118$ Å^3. There is an uncertainty of 20% in each χ parameter, which they attributed to the uncertainty in the molar mass determination [30]. These parameters were obtained by performing experiments within the temperature range of 117 °C $< T <$ 282 °C [30, 35]. As mentioned earlier, PI-PS is the most studied system among the three diblocks, and consequently, several other studies have also reported estimates for χ_{IS} using mean-field theory (Fig. 1). However, since we are using the other two χ_{ij} parameters from Frielinghaus *et al.*, we decide to use the χ_{IS} parameter from the same study for internal consistency.

2.2. Approach 2: χ from Simulation Results

In this method, we estimate the interaction parameters by fitting the experimentally measured values of T_{ODT} for symmetric and nearly-symmetric diblocks to the predicted order–disorder transition obtained from a suite of coarse-grained molecular simulations [38, 39]:

$$\chi N_{\mathrm{ODT}} = 10.5 + \frac{41.0}{\bar{N}^{1/3}} + \frac{123.0}{\bar{N}^{0.56}}, \tag{4}$$

where $\bar{N} = N b_{\mathrm{avg}}^6 / v_{\mathrm{ref}}^2$ is the invariant degree of polymerization and b_{avg} is the average statistical segment length b of the two blocks. The second term in Eq. (4) is the result of Fredrickson–Helfand theory, which was the first theory accounting for the fluctuations effects in symmetric diblock copolymers [44]. Subsequent theoretical studies have shown that the Fredrickson–Helfand theory is applicable to $\bar{N} \gtrsim 10^4$, and gives inaccurate results for $\bar{N} \lesssim 10^4$ [45]. Since most experimental systems lie within the range $200 < \bar{N} < 10000$, Fredrickson–Helfand theory is not optimal for estimating the interaction parameters. The third term in Eq. (4) represents the correction to the Fredrickson–Helfand theory estimated by performing

Table 1: Molecular parameters and the T_{ODT} values reported in the literature for nearly-symmetric samples of the three diblock copolymers: PI-PS, PS-PEO, and PI-PEO. The molecular weight (M_{w}) listed for entries that do not have Đ values corresponds to the number-average molecular weight (M_{n}).

PI-PS							
Name	f_{PS}	M_{w} or M_{n}	Đ	$T_{\mathrm{ODT}}(^{\circ}\mathrm{C})$	N	$\bar{N}$	Reference
IS6	0.46	13.0	1.05	78	136	507	Lin and Balsara [28]
IS7	0.46	14.4	1.05	84	150	562	Lin and Balsara [28]
IS54	0.46	17.0	-	124	187	697	Khandpur *et al.* [29]
IS1	0.54	20.7	1.03	117	218	770	Frielinghaus *et al.* [35]
IS2	0.56	28.9	1.04	200	301	1047	Frielinghaus *et al.* [35]
	f_{PS}			PS-PEO			
SEO11	0.48	13.7	1.04	107.5	194	662	Teran and Balsara [46]
SEO1	0.50	17.0	-	172	251	826	Frielinghaus *et al.* [36]
SEO2	0.49	24.2	-	280	357	1196	Frielinghaus *et al.* [36]
	f_{PI}			PI-PEO			
IO1	0.50	4.4	1.06	132	62	517	Frielinghaus *et al.* [35]
IO2	0.49	7.4	1.10	247	101	849	Frielinghaus *et al.* [35]

large-scale molecular dynamics simulations of various bead-spring models spanning a wide range, $\bar{N} = 100 - 7600$ [38]. Overall, Eq. (4) should be a reliable prediction of χN_{ODT}, especially for the $\bar{N}$ values considered here, and thus is expected to yield reasonably accurate estimates of the interaction parameters [43, 39].

Table 1 lists the specifications of various experimentally synthesized symmetric and nearly-symmetric diblock copolymers reported in literature for the three binary pairs: PI-PS, PS-PEO, and PI-PEO. For an AB diblock copolymer, if the block molecular-weights M_A and M_B are known, then N is calculated as

$$N(T) = \frac{M_A}{\rho_A(T) N_{\mathrm{Av}} v_{\mathrm{ref}}} + \frac{M_B}{\rho_B(T) N_{\mathrm{Av}} v_{\mathrm{ref}}}, \tag{5}$$

where $\rho_A(T)$ and $\rho_B(T)$ are the densities of the monomer types A and B, respectively, at a temperature T, and N_{Av} is the Avogadro's constant. Instead of individual molecular weights, if the overall molecular weight M

is given, then

$$N(T) = \frac{M/(N_{\mathrm{Av}} v_{\mathrm{ref}})}{\rho_A(T) f_A + \rho_B(T) f_B}, \tag{6}$$

where f_A and f_B are the volume fractions of the blocks A and B, respectively. Furthermore, the average statistical segment length is calculated as $b_{\mathrm{avg}} = (f_A b_A^2(T) + f_B b_B^2(T))^{1/2}$, where b_A and b_B are the statistical segment lengths (SSLs) of the blocks A and B, respectively, at a temperature T. We use the temperature-dependent forms of the densities and SSLs because we choose a different reference temperature for different cases depending upon the range of T_{ODT} values in each case. The functional forms for the densities are

$$\rho_I[\mathrm{g/cm^3}] = 0.998 - 1.2 \times 10^{-3} T, \tag{7}$$

$$\rho_S[\mathrm{g/cm^3}] = 1.0865 - 6.19 \times 10^{-4} T + 1.36 \times 10^{-7} T^2, \tag{8}$$

$$\rho_O[\mathrm{g/cm^3}] = 1.139 - 7.31 \times 10^{-4} T, \tag{9}$$

respectively, where T is in °C [46, 47]. The values of SSLs depend on the reference volumes, so we will report their functional form and values once we have decided on a reference volume for a given χ_{ij}. Below, we provide the calculation details for each of the three diblocks separately.

2.2.1. PI-PS

Although the PI-PS diblock copolymer has been studied extensively, there are few studies focusing on symmetric or nearly-symmetric copolymers that report all the information required to obtain the interaction parameter using Eq. (4). Table 1 lists the T_{ODT} values of five nearly-symmetric ($f_I = 0.5 \pm 0.06$) PI-PS diblock copolymers. In order to calculate the parameters N and $\bar{N}$, we select the reference temperature $T = 81$ °C as the average of the T_{ODT} values for IS6 and IS7 listed in Table 1. For this reference temperature, Eqs. (7) and (8) yield $\rho_I = 0.90$ g/cm^3 and $\rho_S = 1.04$ g/cm^3. The reference volume is calculated as the geometric mean of the monomer volumes of PI and PS, $v_{\mathrm{ref}} = \sqrt{v_S v_I} = 157$ Å^3, based on the reported molecular weights of PI and PS repeat units [47]. For the above reference volume, the SSLs of PI and PS are $b_I = \exp[(1/2)(0.00040(T + 273) + 3.77)]$ Å and $b_S = \exp[(1/2)(0.00044(T + 273) + 3.52)]$ Å, respectively, with T in °C [47, 40], which yield $b_I = 7.07$ Å and $b_S = 6.28$ Å at the selected reference temperature. Using the values of N and $\bar{N}$ listed in Table 1 and

fitting to Eq. (4), the interaction parameter χ_{IS} is

$$\chi_{IS} = \frac{111.45}{T} - 0.1852. \tag{10}$$

2.2.2. PS-PEO

In the case of the PS-PEO system, two studies in the literature have reported a total of three T_{ODT} values for the symmetric or nearly-symmetric diblock copolymers (Table 1). We choose the reference temperature for this system as $T = 107.5$ °C, which is the T_{ODT} for the SEO11 sample listed in Table 1. Consequently, Eqs. (8) and (9) yield $\rho_S = 1.02$ g/cm^3 and $\rho_O = 1.06$ g/cm^3, respectively. Similar to the previous case, the reference volume is selected as the geometric mean of the block repeat unit volumes, $v_{\mathrm{ref}} = \sqrt{v_S v_O} = 108$ Å^3. For the selected reference volume and temperature, the values of the SSLs are $b_S = 4.87$ Å, and $b_O = 6.61$ Å, calculated using $b_S = \exp[(1/2)(0.00044(T + 273) + 3.00)]$ Å and $b_O = \exp[(1/2)(0.00023(T + 273) + 3.69)]$ Å, respectively, with T in °C [47]. Using a fit to Eq. (4), the interaction parameter χ_{SO} is estimated as

$$\chi_{SO} = \frac{58.81}{T} - 0.0602. \tag{11}$$

2.2.3. PI-PEO

The PI-PEO diblock copolymer is the least studied system among all the three diblocks. We found only one report that provides all the information required to obtain the χ parameter using Eq. (4) [35]. This study reports two T_{ODT} values for the symmetric or nearly-symmetric PI-PEO diblock samples. Although the resulting estimate of χ is expected to have significant uncertainty, we nonetheless chose to obtain the interaction parameter using the two available data points. We select the reference temperature $T = 140$ °C, which yields $\rho_I = 0.83$ g/cm^3, and $\rho_O = 1.04$ g/cm^3 using Eqs. (7) and (9), respectively. The reference volume for this case is $v_{\mathrm{ref}} = \sqrt{v_I v_O} = 117$ Å^3. For the chosen reference volume, $b_I = \exp[(1/2)(0.0004(T + 273) + 3.43)]$ Å, and $b_O = \exp[(1/2)(0.00023(T + 273) + 4.0)]$ Å [47], which yield $b_I = 6.00$ Å, and $b_O = 7.75$ Å, respectively, at $T = 140$ °C. The corresponding values of N and $\bar{N}$ are listed in Table 1. Using a fit to Eq. (4), the interaction parameter χ_{IO} is

$$\chi_{IO} = \frac{250.84}{T} - 0.3077. \tag{12}$$

Collectively, Eqs. (10), (11) and (12) form the set of binary interaction parameters that is obtained in this approach, i.e., by fitting the experimental values of T_{ODT} to the results of molecular simulations. Note that the reference volume used to calculate the molecular parameters given in Table 1 differs among the three diblocks. Transforming the above χ parameters to a common reference volume, $v_{\mathrm{ref}} = 118$ Å^3, yields

$$\chi_{IS} = \frac{83.76}{T} - 0.1392, \tag{13}$$

$$\chi_{SO} = \frac{64.26}{T} - 0.0658, \tag{14}$$

$$\chi_{IO} = \frac{252.98}{T} - 0.3103. \tag{15}$$

2.3. Approach 3: χ from Renormalized One-Loop (ROL) Theory

In this approach, the χ parameters are estimated using another fluctuation-based model, the renormalized one-loop (ROL) theory. The ROL theory for diblock copolymers was developed by Morse and coworkers [41] in 2011 and is by far the most accurate theory of the composition fluctuations in the disordered phase of symmetric and nearly-symmetric diblock copolymers. It provides accurate predictions for the complete structure-factor function, $S(q)$ vs q, as well as the variations of peak position q^* and peak intensity $S(q^*)$ as functions of Flory–Huggins interaction parameter χ_{ij}. The mathematical tools underlying ROL theory are difficult to apply to ordered structures; hence, the theory does not provide any predictions for χN_{ODT} or the properties of the ordered structures. This is the sole reason that this third approach, in contrast to the previous two approaches, uses structure factor data to obtain the Flory–Huggins parameters.

The overall procedure to obtain the interaction parameters using ROL theory involves three steps. In the first step, the values of peak intensities $I(q^*)$ are obtained at different temperatures from the SAXS and SANS experimental results reported in the literature. The second step involves transforming these values to the normalized inverse peak structure factor $cNS^{-1}(q^*)$, where $c = 1/v_{\mathrm{ref}}$. In the final step, the temperature dependence of $cNS^{-1}(q^*)$ obtained in the previous step is fitted to the $cNS^{-1}(q^*)$ vs χ_{ij} function predicted by the ROL theory to estimate the parameters α_{ij} and β_{ij} in $\chi_{ij} = \alpha_{ij}/T + \beta_{ij}$. We emphasize here that this whole procedure is quite intricate and requires solving the set of highly non-linear ROL equations numerically (third step). Pavani Medapuram estimated two of

the interaction parameters that are required in this work, χ_{IS} and χ_{SO}, as a part of her doctoral work. Hence, we use the two interaction parameters from her PhD thesis [39]:

$$\chi_{IS} = \frac{95.50}{T} - 0.1578, \tag{16}$$

$$\chi_{SO} = \frac{45.04}{T} - 0.0295. \tag{17}$$

The above interaction parameters correspond to the reference volume, $v_{\mathrm{ref}} = 118$ Å^3. As PI-PEO is the least studied system, we were unable to identify even a single study in the literature that reports SAXS or SANS intensities for the symmetric or nearly-symmetric PI-PEO diblocks. Due to unavailability of the required data, we chose to use the χ_{IO} estimate from the fit to simulation results (the second approach) to perform the SCFT calculations for this last approach. Consequently, Eqs. (15)-(17) together constitute the set of interaction parameters for this third approach.

2.4. Comparison of Different Methods

Before considering the outcome of the SCFT calculations, it is instructive to compare the estimates of χ_{ij} obtained from the different methods to appreciate the extent of the differences between them. Figure 2a, b, and c compare the χ_{IS}, χ_{SO}, and χ_{IO} parameters, respectively, obtained using the methods outlined above. It is interesting that the estimates of χ_{IS} obtained using the fluctuation-based methods are quite similar, and differ significantly from that obtained using mean-field theory. However, the same is not true for χ_{SO}; estimates obtained from the mean-field theory and simulations predictions are similar and differ noticeably from that obtained using ROL theory.

The two fluctuation-based methods used here are fundamentally equivalent. The estimation of χN_{ODT} from molecular simulations, i.e., Eq. (4), requires the transformation of interaction-potential parameters in simulations to the appropriate χ parameter. Such a transformation is performed by fitting the structure factor calculated from simulations to that predicted by ROL theory [38, 40, 43]. Hence, if both, the structure factor and the T_{ODT} data of a system are available under same conditions with negligible uncertainty, and if the system is monodisperse, then Approaches 2 and 3 should yield the same χ vs. T estimate. The differences between the estimates of Approaches 2 and 3 depicted by Fig. 2 stem from the uncertainties in

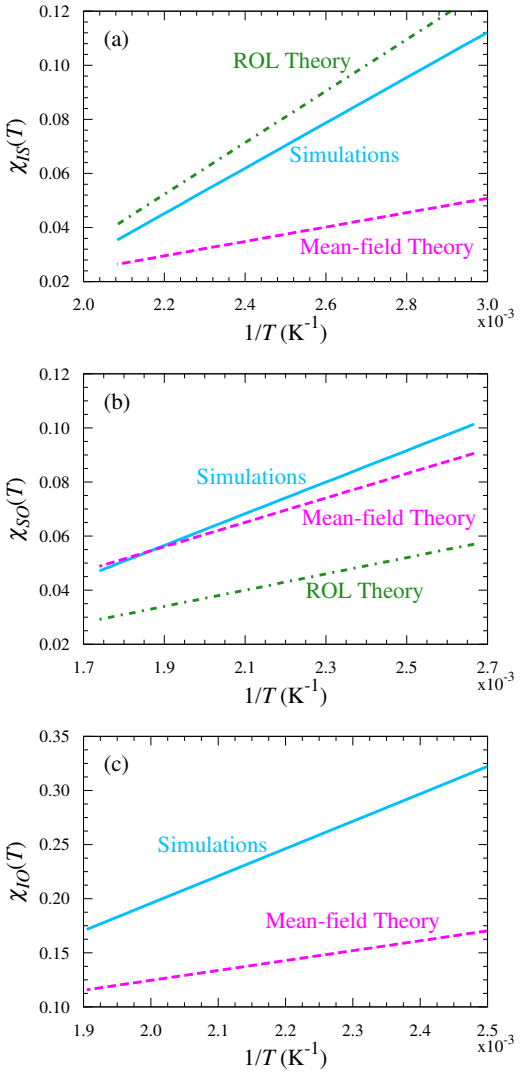

Figure 2: Comparison of Flory–Huggins interaction parameters, (a) poly(isoprene) and poly(styrene), χ_{IS}, and (b) poly(styrene) and poly(ethylene oxide), χ_{SO}, obtained using the three methods: mean-field theory, simulations results, or renormalized one-loop (ROL) theory. (c) Comparison of poly(isoprene) and poly(ethylene oxide) interaction parameter, χ_{IO}, estimated using mean-field theory and simulations results.

the experimental measurements among different groups and due to the polydispersity of the sample. Nevertheless, for the purpose of this study, i.e., to examine the sensitivity of phase behavior towards different χ vs.

T estimates, both approaches serve as equally good methods even if they yield different sets of χ parameters.

3. SCFT Calculations

SCFT and its numerical implementation are discussed in great detail in many previous studies [20, 21, 22]. Hence, we discuss only the necessary ingredients and parameters required for the calculations reported here. We use the open-source package polymer self-consistent field (PSCF) to perform all the SCFT calculations, and direct interested readers to Ref. 22 for the details regarding the numerical algorithms and features of PSCF.

Briefly, PSCF is based on a unit-cell implementation of SCFT, hence, a list of all the possible candidate structures is required *a priori* to examine the phase behavior [22]. Based on the experimental results on SIS′O tetrablocks [34], we consider six candidate ordered structures: five sphere-forming phases [body-centered cubic (BCC), face-centered cubic (FCC), hexagonal close-packed (HCP), Frank-Kasper σ and A15], along with hexagonally-packed cylinders (HEX_C). For each of these six phases, we construct the required guess structures to begin the iteration procedure following the reciprocal-space initialization approach developed in our earlier work [22]. Furthermore, we use two different types of iteration algorithms, Newton–Raphson and Anderson mixing, depending on the their respective advantages in simulating the types of structures considered in this work [22, 48]. All the other numerical parameters, including the continuation method implemented by the SWEEP feature, which is used extensively in this study, are discussed in our earlier work [22]. We emphasize that SCFT yields the free energies of different ordered structures, which are then compared to one another to construct the phase diagram. SCFT does not provide any information about the nucleation and growth dynamics of the ordered structures that may govern non-equilibrium phase behavior.

Within the SCFT framework, the phase behavior of linear SIS′O tetrablocks is determined by the six molecular parameters: $f_I, f_O, f_S, b_I/b_S, b_O/b_S$ and N, and three interaction parameters: χ_{IS}, χ_{IO}, and χ_{SO}. Since we are interested in examining the effect of the temperature-dependence of the χ parameters alone on the SCFT-predicted phase behavior, we assume the other parameters are temperature invariant. Specifically, for all the SCFT calculations reported here, we calculate N based on a common reference

volume $v_{\text{ref}} = 118$ Å^3, and use the temperature-independent SSLs, $b_I = 6.0$ Å, $b_S = 5.4$ Å, and $b_O = 7.8$ Å for PI, PS, and PEO, respectively. It has been shown previously that the precise values of SSLs with $\Delta b = 0.2$ Å are crucial when the results from SCFT and experiments are compared for some of the detailed features such as interfacial thickness and domain spacing [49]. However, for comparing the phase transitions and overall morphological behavior, usually a significant amount of disparity between the SCFT-input and experimentally-reported SSL values is observed [4, 50, 51, 52]. Note that the maximum variation in the SSLs for the temperature range considered here is small, $\Delta b_I \approx 0.08$ Å, $\Delta b_S \approx 0.05$ Å, and $\Delta b_O \approx 0.03$ Å. Hence, our assumption of temperature-independent SSLs is reasonable and is not expected to have a pronounced effect on the results.

In our earlier work on SIS′O tetrablocks [34], we identified that the difference in the lengths of the PS and PS′ blocks, $\tau = N_S/(N_S + N_{S'})$, plays an important role in governing the phase behavior and the tetrablock with $\tau = 0.73$, referred to as SIS′O-0.73 in Ref. 34, exhibited the richest phase behavior when compared to tetrablocks with other τ values. Thus we focus here on the SIS′O-0.73 tetrablock and perform all our calculations in a way that mimics the experimental synthesis; increasing f_O implies adding the desired length of the PEO block to the parent SIS′ triblock of constant length $N_{SIS'} = 298$ along a constant isopleth $f_I/(f_S + f_{S'}) = 0.5$. Consequently, the overall N is calculated as a function of f_O as

$$N = \frac{298}{1 - f_O}. \tag{18}$$

For a typically synthesized SIS′O sample [34], the value of $N \approx 350$ and the segregation strengths at $T = 150$ °C using the interaction parameters given in Eqs. (13)-(15) are $\chi N_{IS} \approx 20$, $\chi N_{SO} \approx 30$, and $\chi N_{IO} \approx 100$.

The selection of the SIS′O-0.73 tetrablock reduces the dimension of the parameter space to four: $f_O, \chi_{IS}, \chi_{IO}$, and χ_{SO}. Using the χ_{ij} vs T functions obtained in the previous section, we examine the phase behavior in the $T - f_O$ plane and compare SCFT predictions with experiments. The different phases for SIS′O-0.73 are observed in experiments within the temperature range of 160 °C $< T <$ 280 °C before the sample disorders at $T_{\text{ODT}} \approx 285$ °C. Preliminary SCFT calculations on SIS′O-0.73 suggested that the order–disorder transition predicted by SCFT is $T_{\text{ODT}} \approx 220$ °C. Hence, throughout this work, we examine the phase behavior within the temperature range of 140 °C $< T <$ 180 °C and for a wide range of volume

fraction, $0.05 \leq f_O \leq 0.30$. This corresponds to the following ranges of the volume fractions of the other three blocks:

$$0.3468 \geq f_S \geq 0.2555, \tag{19}$$

$$0.4750 \geq f_I \geq 0.3500, \tag{20}$$

$$0.1283 \geq f_{S'} \geq 0.0945. \tag{21}$$

Moreover, the experimentally synthesized SIS′O-0.73 sample has a polydispersity $Đ = 1.03$, which, in addition to few other molecular parameters, is subjected to small uncertainties (see Section S4 in Supplementary Material). In this work, we neglect such uncertainties, and perform all our calculations for a monodisperse melt.

4. Predicted Phase Behaviors and Morphologies

4.1. Overall Trends

Figure 3 shows the phase behavior predicted by SCFT in the $T - f_O$ plane using the interaction parameters estimated from Approaches 1, 2, and 3, respectively. The dashed (black) line at $f_O = 0.13$ in Fig. 3 denotes the PEO volume fraction of the experimentally synthesized sample, SIS′O-0.73. It is clear from Fig. 3 that the phase behavior is extremely sensitive to the Flory–Huggins interaction parameters. This sensitivity is best highlighted by comparing Figs. 3b and c, which correspond to SCFT results obtained using the χ parameters estimated using the fluctuation-based theories. Among these two sets of parameters, only the parameter χ_{SO} is significantly different, with χ_{IS} being almost same (see Fig. 2a) and χ_{IO} exactly the same since we were unable to identify experimental data to use with ROL theory. Nevertheless, the phase behavior depicted in Fig. 3b is very different from that shown in Fig. 3c.

It is worthwhile to examine whether SCFT predicts the expected shapes of the particles and arrangement of the blocks. In SIS′O tetrablocks, $\chi_{IO} \gg \chi_{SO} \gtrsim \chi_{IS}$, hence, they are expected to form domain structures that minimize the unfavorable PI/PEO contacts. Figure 4a shows the density profiles within the unit cell for all six ordered structures. All of the structures contain well defined core-shell particles in which the PEO block (yellow) forms the core and the PS′ block (blue) forms the shell to screen the contacts between PEO and PI. Figure 4b shows the monomer concentration profiles $\phi(r)$ for one of the structures, the BCC phase along the body diagonal

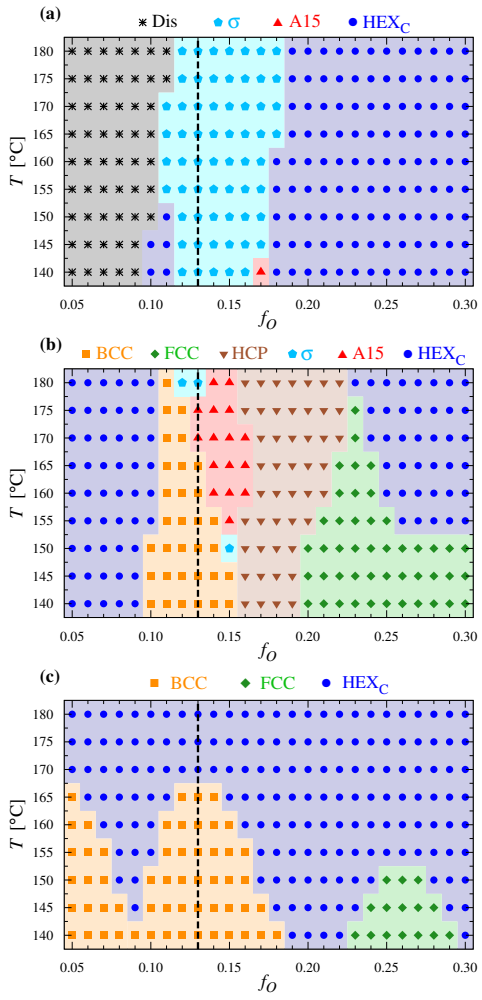

Figure 3: SCFT-calculated phase diagrams in the $T - f_{\mathrm{O}}$ plane using the interaction parameters reported in (a) Approach 1, i.e., Eqs. (1)-(3) (χ_{ij} estimated using mean-field theory), (b) Approach 2, i.e., Eqs. (13)-(15) (χ_{ij} estimated using simulation results), and (c) Approach 3, i.e., Eqs. (15)-(17) (χ_{ij} estimated using ROL theory). These calculations are done for the SIS′O tetrablock terpolymer having $\tau = N_{\mathrm{S}}/(N_{\mathrm{S}} + N_{\mathrm{S}'}) = 0.73$ and $f_{\mathrm{I}}/(f_{\mathrm{S}} + f_{\mathrm{S}'}) = 0.50$, and performed in a manner that mimics the experimental synthesis; increasing f_{O} implies adding the corresponding length of the PEO block to the parent SIS′ triblock of constant length $N_{\mathrm{SIS}'} = 298$ [34]. The dashed (black) line denotes the experimentally synthesized SIS′O-0.73 tetrablock having $f_{\mathrm{O}} = 0.13$.

([111]), confirming the core-shell nature of the particles. In Fig. 4b, it is important to note that the PI and PS blocks are intermixed significantly

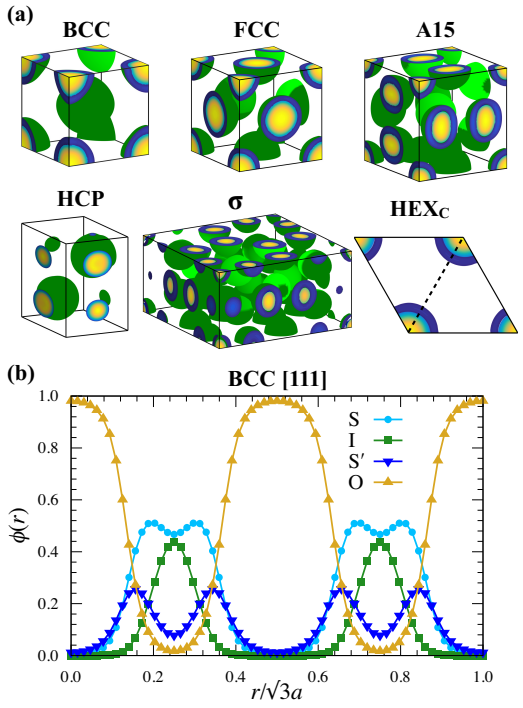

Figure 4: Density profiles within the unit cells of different sphere-forming phases considered in this work. The unit-cell representations depict the density profiles of the PEO block forming the discrete microdomains (yellow) with PS′ forming a shell around it (blue), while the density profiles of the PI and PS blocks are omitted for clarity. These profiles are calculated from the converged solutions obtained at $T = 180$ °C and $f_O = 0.13$ using the simulation-results-fitted interaction parameters given in Eqs. (10)-(12). (b) The density profiles of all the four blocks along the [111] direction in the BCC phase, depicting the core-shell nature of the particles.

within the matrix. In previous work, we hypothesized that the mixing of blocks within the matrix has a profound influence on the relative stability of different phases, particularly the complex phases [34]. The actual arrangement of the blocks is not obvious in Fig. 4b, however, it is reasonable to assume that a fraction of the chains will have their terminal PS and PI blocks dangling and mixed within the matrix, while the rest of the chains may bridge between different particles or loop back within the same particle [53].

While performing the calculations for Figs. 3b and c, we found multiple converged solutions having different free energies at same state point. Fig-

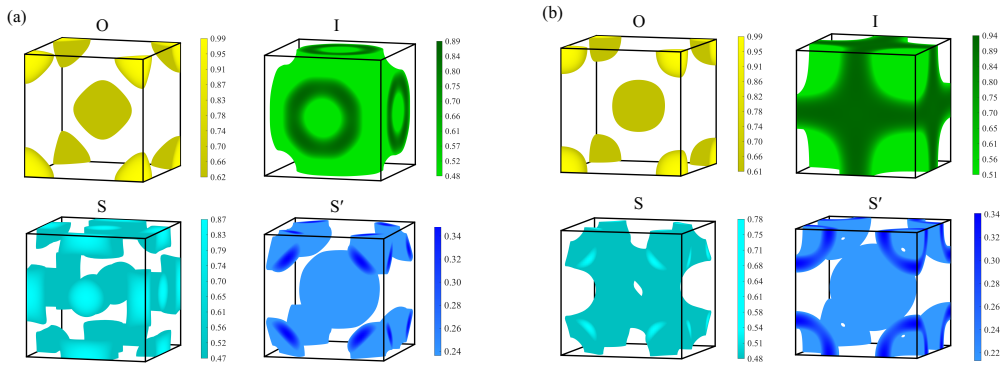

Figure 5: Comparison of the block density profiles of two converged solutions at $f_O = 0.13$ and $T = 140$ °C obtained using different guess structures. The structure in (a) is obtained using the converged solution of ($f_O = 0.14, T = 140$ °C), while the structure in (b) is obtained using the converged solution of ($f_O = 0.13, T = 141$ °C). Relative free energies per chain of the two structures are (a) $F - F_{\text{Dis}}/k_{\text{B}}T = -7.9677$, and (b) $F - F_{\text{Dis}}/k_{\text{B}}T = -7.9081$. Both the solutions are obtained using the Newton-Raphson iteration algorithm.

ure 5 shows the density profiles of the four blocks within the BCC phase for the two converged solutions at ($T = 140$ °C, $f_O = 0.13$) obtained using different guess structures. Interestingly, the shape of the PEO particles differs significantly among the two solutions. This difference in the shapes arises due to entirely different segregation of the PI and PS blocks within the matrix. Moreover, during the numerical continuation of solutions in the parameter space, the solution branch corresponding to Fig. 5(a) experiences a discontinuity in the unit-cell dimension, which results into a significantly different structure and free energy (see Fig. S1 in Supplementary Material). Such behavior is also observed with the FCC and HCP phases at low temperatures in the phase diagram of Approach 2 (see Figs. S2-S4 in Supplementary Material). The ability of multiblock polymers to produce different structural features while maintaining the prescribed crystallographic symmetry and position of the particles highlights an additional level of complexity involved in modeling these materials. Nonetheless, in constructing the phase diagrams shown in Fig. 3, we consider the structure that have the least free energy among all the multiple converged solutions.

Experimentally, SIS′O-0.73 exhibited different phase-transition sequences on heating and cooling, as seen in Fig. 8 of Ref. [34]. Heating the sample from a freeze-dried state at $T = 120$ °C yielded the transition HCP+FCC $\rightarrow$ A15 $\rightarrow \sigma \rightarrow$ Dis, while cooling the disordered material produced the

transition Dis $\rightarrow$ BCC(transient) $\rightarrow \sigma \rightarrow$ HCP, with BCC observed as a transient phase before the growth of σ begins. Another phase transition sequence that involves a liquid-like packing of particles and dodecagonal quasicrystalline morphology is observed when heating the freeze-dried sample starting at a reasonably high temperature ($T = 260$ °C) [34], but we will not discuss this transition as we are not considering the quasicrystalline structures in this work. It is important to note that the morphological behavior observed in SIS′O-0.73 is path-dependent. For example, the A15 phase is not observed on cooling but only on heating, and that too when heating is started at a very low temperature. Such processing-dependent phenomena cannot be captured by an equilibrium theory like SCFT. Nevertheless, it is worthwhile to determine if there is any correspondence between the SCFT results and experiments. We thus proceed to examine the results of each method in more detail.

4.2. Approach 1

The phase behavior depicted in Fig. 3a, obtained using the mean-field theory estimates of χ, predicts only two sphere-forming structures as the stable phases: σ and A15, with A15 occupying a tiny region at low temperatures. More noticeably, there is no phase transition predicted for SIS′O-0.73, with only σ as the stable phase. Even at other volume fractions, there are not many phase transitions with the phase boundaries appearing almost vertical and thus invariant with temperature. Interestingly, the phase diagram in Fig. 3a looks similar to that of an AB diblock, where f_O, analogous to f_A, controls the domain curvature; decreasing f_O transforms cylinders to spheres at a constant temperature. However, by varying f_O, the value of N changes by Eq. (18). Consequently, the segregation strengths, χN_{IS}, χN_{SO}, and χN_{IO}, also change. Hence, the phase diagram in the $T - f_O$ plane is not precisely the same as that in the $\chi N - f_A$ plane typically used to examine the phase behavior of AB diblocks.

Overall, it is clear that the mean-field theory set of interaction parameters does not predict the phase behavior observed experimentally, which is unsurprising. It is important to note that the diblock samples synthesized by Frielinghaus *et al.* [35, 36] to obtain these parameters are of moderate molecular weights, $N \sim 100 - 300$, and consequently correspond to moderate values of $\bar{N}$ (see Table 1). For such values of $\bar{N}$, the fluctuation effects near the order–disorder transition become increasingly important and shift χN_{ODT} to a value significantly higher than the mean-field-theory prediction

of 10.5 [54, 55]. This is a likely reason for the inability of the SCFT calculations using χ parameters obtained from the mean-field T_{ODT} prediction to capture the experimentally observed phase behavior.

4.3. Approach 2

In contrast, the phase diagram shown in Fig. 3b, obtained using the Flory–Huggins parameters estimated by fitting T_{ODT} to simulations, is very rich, exhibiting all six of the different ordered structures. For the SIS′O-0.73 sample, denoted by the dashed line at $f_{\mathrm{O}} = 0.13$ in Fig. 3b, the phase transition on heating is BCC $\rightarrow$ A15 $\rightarrow \sigma$. The phase transition predicted by SCFT for SIS′O-0.73 does not match exactly with experiments.

In Fig. 3b, the close-packed structures HCP and FCC do not appear to be stable for SIS′O-0.73. Instead, we observe the BCC phase at low temperatures. However, it is remarkable that both of the complex phases, σ and A15, are predicted to be stable phases at high temperatures. Recently, Liu *et al.* [53] reported extensive SCFT calculations to examine the stability of complex phases in ABAC tetrablocks, considering network structures also as candidate phases. They found that A15 always exists as a metastable phase, with a free energy consistently higher than that of the σ phase for various regions of the parameter space explored in their study (see Figs. 8-10 in Ref. 53). However, here we observe A15 to be the stable phase. There are two reasons for this seemingly contrasting result. The first obvious reason is that the SCFT parameters, in particular the segregation strengths, used in their study are noticeably different from those corresponding to any of the phase diagrams shown in Fig. 3. Specifically, they have used $\chi N_{IS} = 11.0, \chi N_{SO} = 14.2$, and $\chi N_{IO} = 45.8$, while we have $\chi N_{IS} = 17.1, \chi N_{SO} = 27.2$, and $\chi N_{IO} = 89.3$ for SIS′O-0.73 at $T = 170$ °C using Approach 2. The second reason is that since we are primarily interested in comparing SCFT predictions to experiments, we have done calculations that resemble the experimental synthesis, while the calculations reported by Liu *et al.* are not done with such a restriction. Nevertheless, Fig. 3b shows the phase transition A15 $\rightarrow \sigma$ on heating, which is the same as that observed experimentally between these two phases, suggesting that this set of parameters is moderately close in accurately modeling the interactions in SIS′O system. In comparison to the phase diagram of Fig. 3a, it is certain that the use of fluctuation-based prediction of χN_{ODT} is a more accurate way to estimate the χ parameters.

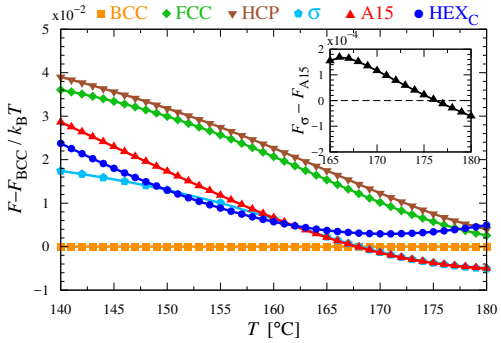

Figure 6: Free energies per chain of different phases relative to that of the BCC phase, $F - F_{BCC}/k_BT$, along the dashed (black) line shown in Fig. 3b. The inset shows the difference in the free energies of the σ and A15 phases at high temperatures, i.e., 160 °C $<$ T $<$ 180 °C.

Figure 6 shows the temperature-dependent free energies per chain of different phases relative to that of the BCC phase for the SIS′O-0.73 sample using the χ parameters obtained in Approach 2, i.e., along the dashed line shown in Fig. 3b. In general, we see that the difference in the free energies between any two phases lies within the range $10^{-2}\ k_BT$ to $10^{-3}\ k_BT$. However, the difference between the free energies of σ and A15 reduces to the order of $10^{-4}\ k_BT$ for a wide temperature range, 160 °C $<$ T $<$ 180 °C, as depicted in the inset of Fig. 6. This is similar to the difference observed for these two phases in diblock copolymers [3]. In addition to complex phases, as expected, the free energy difference between the two close-packed structures is also very small. Such tiny differences in the free energies are consistent with our argument that the phase behavior is very sensitive to the interaction parameters used for the SCFT calculations. Moreover, such narrow differences in the free energies are not limited to SIS′O-0.73 ($f_O = 0.13$) sample, but persist over almost the entire phase diagram (see Fig. S5 in Supplementary Material).

One of the interesting features to note in the phase diagram of Fig. 3b is that the HEX_C phase is stable under two separate conditions, one at significantly low f_O values and the other at high f_O values. The formation of cylinders at such low volume fractions of the PEO block contrasts with the typical morphological behavior observed in diblock polymers since the low volume fraction of the core block has a tendency to produce sphere-forming morphologies. Figure 7 shows the density profiles along the [110]

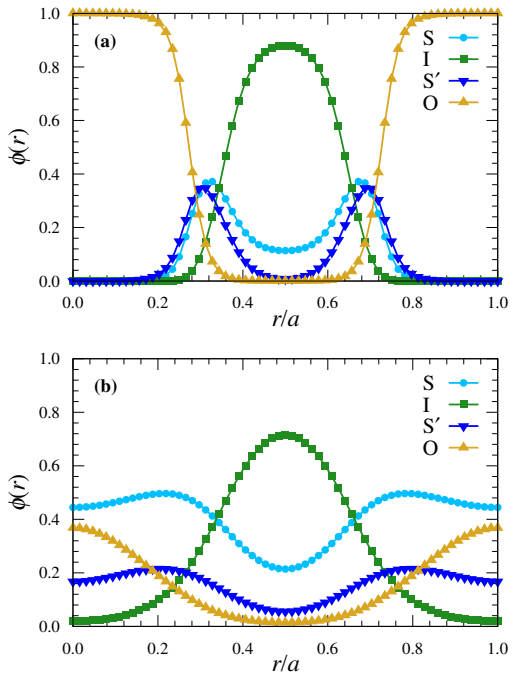

Figure 7: Density profiles of different blocks along the [110] direction (dashed line in Fig. 3a) within the unit cell of the HEX_C phase. These profiles are computed for (a) $f_O = 0.28$, and (b) $f_O = 0.08$ at $T = 170$ °C using the simulations-results-fitted parameters corresponding to the phase diagram shown in Fig. 3b.

direction for the two HEX_C phases in Fig. 3b obtained at $f_O = 0.28$ and $f_O = 0.08$, respectively, for $T = 170$ °C. For $f_O = 0.28$, the structure contains moderately segregated core-shell cylinders, consistent with Fig. 4. However, no shell forms at $f_O = 0.08$. Instead, the core of the cylinder is formed jointly by the PEO, PS′, and PS blocks. Moreover, the significantly high density of the terminal PS block at $r/a = 0$ in Fig. 7b suggests that in this case a large fraction of the chains are looping back within the same particle to aid the formation of cylinders. We emphasize that the calculations for the HEX_C phase are done in two dimensions constraining the calculation to have *P6mm* symmetry. Hence, it is not clear whether the HEX_C phase is comprised of infinitely long cylinders. It is possible that the HEX_C region at low volume fractions resembles a structure comprising of spherical particles arranged in a three-dimensional hexagonal lattice, similar to the morphology referred to as HEX_S in Ref. 34.

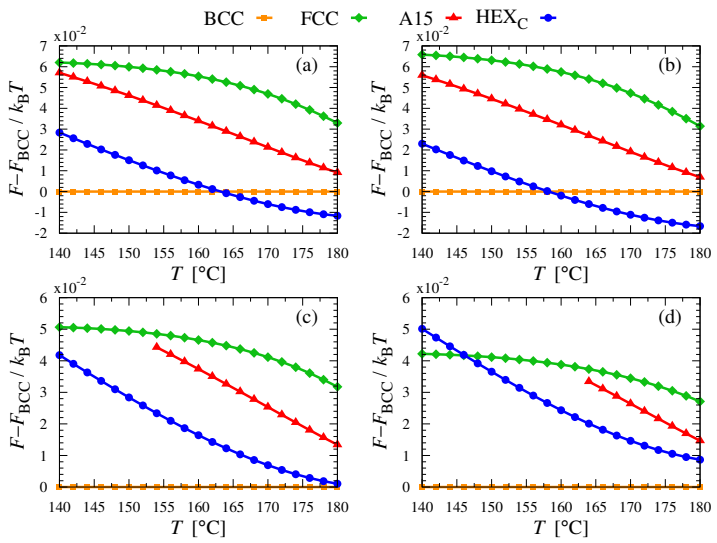

Figure 8: Relative free energies per chain, $F - F_{BCC}/k_BT$, along the dashed (black) line shown in Fig. 3c (Approach 3) for four different cases having χ_{IO} (a) increased by 10%, (b) increased by 20%, (c) decreased by 10%, and (d) decreased by 20%, from the estimate given by Eq. (12).

4.4. Approach 3

The phase diagram corresponding to the interaction parameters obtained using ROL theory, shown in Fig. 3c, exhibits two sphere-forming structures (BCC and FCC) while most of the phase space is occupied by the HEX$_C$ phase. More importantly, neither of the two complex phases, σ and A15, are predicted to be stable for SIS′O-0.73 throughout the temperature range explored. Instead, SIS′O-0.73 exhibits a transition from BCC to HEX$_C$ on heating, although the HEX$_C$ phase was never observed in experiments (see Fig. S6 in Supplementary Material for HEX$_C$-BCC boundary). Note that this set of χ parameters is also estimated using a fluctuation-based theory, hence, expected to predict the phase behavior in close agreement with experiments, similar to that of Approach 2 (Fig. 3b). However, the resulting parameters and SCFT calculations failed to capture some of the important features observed experimentally.

Recall that the interaction parameter χ_{IO} in this approach is same as that of Approach 2. Since the phase diagram of this approach is significantly different than that of Approach 2 and does not predict any of the complex phases observed experimentally, it is worth examining the effect of variation

in χ_{IO} given by Eq. (12) on the phase behavior depicted in Fig. 3c. Figure 8 shows the relative free energies per chain, $F - F_{\mathrm{BCC}}/k_{\mathrm{B}}T$, along the dashed line (SIS′O-0.73) shown in Fig. 3c for four cases having χ_{IO} increased and decreased by 10% and 20% from the estimate given by Eq. (12). Since the free energy differences between A15 and σ, and between FCC and HCP are very small, we omit simulating the expensive σ and HCP phases for these calculations. It is evident from Fig. 8 that the perturbation of χ_{IO} up to 20% affects only the order–order transition temperature between the BCC and $\mathrm{HEX_C}$ phases while it does not stabilize any new phases for SIS′O-0.73. Nevertheless, the results in Fig. 8 highlight that the set of χ parameters that can model the experimental phase behavior exactly may be significantly different from that obtained in Approach 3.

5. Conclusion

We have examined the sensitivity of the SCFT-predicted phase behavior towards the set of Flory–Huggins interaction parameters for an SIS′O tetrablock terpolymer. We used three different sets of χ parameters obtained by fitting experimental results on diblock copolymers to the predictions of mean-field theory, coarse-grained molecular dynamics simulations, or renormalized one-loop theory. The phase behaviors predicted by each of the three sets of Flory–Huggins parameters differ significantly with one another and none of them captures the experimentally-observed phase behavior comprehensively. Nevertheless, the SCFT calculations using the simulations-results-fitted parameters predict both the complex phases σ and A15 to be the stable phases for the experimentally synthesized SIS′O sample in which these phases were observed. Moreover, using this set of χ parameters in the SCFT calculation predicts the same phase transition sequence between these two phases that is observed experimentally on heating the sample, suggesting that they best describe the SIS′O system among the three sets of parameters studied here.

Overall, our results highlight certain challenges in modeling the phase behavior of multiblock polymers comprising more than one binary interaction parameter. These parameters are typically obtained by performing experiments on diblock copolymers and represent a coarse-grained description of the intermolecular interactions between two chemically distinct monomeric segments. There are two noted shortcomings to this approach. First, such a description neglects interactions that are prevalent below the

statistical segment length, such as hydrogen bonding, that can have a profound influence on the local liquid structure [56]. Monomer shapes [57, 58], thermal expansivities, [59] and equation-of-state effects [60] are also ignored in the coarse-grained description. The treatment of segment-segment interactions in this model is due to contact, and thus does not allow for a finite range of attraction that could further affect the results. Second, Maurer *et al.* [42] have demonstrated that for some cases, the phase behavior of both A/B blends and AB diblock copolymers comprising the same monomer types A and B, cannot be described using a single χ_{AB} vs. T function. This highlights that it may not be possible to model the phase behavior of block polymer quantitatively by using only the Flory-Huggins type interaction parameters. Hence, it may be necessary to employ computationally expensive atomistic simulations if the ultimate goal is to determine the phase behavior comprehensively, predicting all the order–order and order–disorder transitions accurately [25]. Alternatively, one could abandon the approach of obtaining χ_{ij} values for multiblock polymers from their diblock components. Rather, it should be possible to obtain estimates of χ_{ij} for a multiblock polymer by first producing an experimental data set on that polymer's phase behavior, analogous to that obtained in Ref. 34, and then using the χ_{ij} as fitting parameters for the SCFT-predicted phase behavior. While such calculations may be expensive, a recent advance in solving the inverse problem for multiblock polymers [61] presents an enticing approach to resolving this conundrum.

Acknowledgements

The authors gratefully acknowledge helpful discussions with David C. Morse. We also acknowledge the computational resources provided by the Minnesota Supercomputing Institute at University of Minnesota. This work was supported by NSF DMR-1333669 and DMR-1725272.

[1] C. A. Tyler, D. C. Morse, Orthorhombic *Fddd* network in triblock and diblock copolymer melts, Phys. Rev. Lett. 94 (20) (2005) 208302.

[2] S. Lee, M. J. Bluemle, F. S. Bates, Discovery of a Frank-Kasper σ phase in sphere-forming block copolymer melts, Science 330 (6002) (2010) 349–353.

[3] K. Kim, M. W. Schulze, A. Arora, R. M. Lewis, M. A. Hillmyer, K. D. Dorfman, F. S. Bates, Thermal processing of diblock copolymer melts mimics metallurgy, Science 356 (6337) (2017) 520–523.

[4] N. Xie, W. Li, F. Qiu, A.-C. Shi, σ phase formed in conformationally asymmetric AB-type block copolymers, ACS Macro Lett. 3 (9) (2014) 906–910.

[5] F. S. Bates, M. A. Hillmyer, T. P. Lodge, C. M. Bates, K. T. Delaney, G. H. Fredrickson, Multiblock polymers: Panacea or Pandora's box?, Science 336 (6080) (2012) 434–440.

[6] C. Auschra, R. Stadler, New ordered morphologies in ABC triblock copolymers, Macromolecules 26 (9) (1993) 2171–2174.

[7] Y. Mogi, M. Nomura, H. Kotsuji, K. Ohnishi, Y. Matsushita, I. Noda, Superlattice structures in morphologies of the ABC triblock copolymers, Macromolecules 27 (23) (1994) 6755–6760.

[8] W. Zheng, Z.-G. Wang, Morphology of ABC triblock copolymers, Macromolecules 28 (21) (1995) 7215–7223.

[9] F. S. Bates, G. H. Fredrickson, Block copolymers-designer soft materials, Phys. Today 52 (2) (1999) 32–38.

[10] J. Chatterjee, S. Jain, F. S. Bates, Comprehensive phase behavior of poly (isoprene-b-styrene-b-ethylene oxide) triblock copolymers, Macromolecules 40 (8) (2007) 2882–2896.

[11] Z. Guo, G. Zhang, F. Qiu, H. Zhang, Y. Yang, A.-C. Shi, Discovering ordered phases of block copolymers: New results from a generic fourier-space approach, Phys. Rev. Lett. 101 (2) (2008) 028301.

[12] G. Zhang, F. Qiu, H. Zhang, Y. Yang, A.-C. Shi, Scft study of tiling patterns in abc star terpolymers, Macromolecules 43 (6) (2010) 2981–2989.

[13] W. Xu, K. Jiang, P. Zhang, A.-C. Shi, A strategy to explore stable and metastable ordered phases of block copolymers, J. Phys. Chem. B 117 (17) (2013) 5296–5305.

[14] S. Sioula, N. Hadjichristidis, E. L. Thomas, Novel 2-dimensionally periodic non-constant mean curvature morphologies of 3-miktoarm star terpolymers of styrene, isoprene, and methyl methacrylate, Macromolecules 31 (16) (1998) 5272–5277.

[15] T. Gemma, A. Hatano, T. Dotera, Monte carlo simulations of the morphology of ABC star polymers using the diagonal bond method, Macromolecules 35 (8) (2002) 3225–3237.

[16] K. Yamauchi, K. Takahashi, H. Hasegawa, H. Iatrou, N. Hadjichristidis, T. Kaneko, Y. Nishikawa, H. Jinnai, T. Matsui, H. Nishioka, et al., Microdomain morphology in an ABC 3-miktoarm star terpolymer: A study by energy-filtering TEM and 3D electron tomography, Macromolecules 36 (19) (2003) 6962–6966.

[17] K. Hayashida, T. Dotera, A. Takano, Y. Matsushita, Polymeric quasicrystal: Mesoscopic quasicrystalline tiling in ABC star polymers, Phys. Rev. Lett. 98 (19) (2007) 195502.

[18] M. W. Matsen, M. Schick, Stable and unstable phases of a diblock copolymer melt, Phys. Rev. Lett. 72 (16) (1994) 2660–2663.

[19] F. Drolet, G. H. Fredrickson, Combinatorial screening of complex block copolymer assembly with self-consistent field theory, Phys. Rev. Lett. 83 (21) (1999) 4317–4320.

[20] M. W. Matsen, The standard Gaussian model for block copolymer melts, J. Phys.: Condens. Matter 14 (2) (2001) R21.

[21] G. H. Fredrickson, V. Ganesan, F. Drolet, Field-theoretic computer simulation methods for polymers and complex fluids, Macromolecules 35 (1) (2002) 16–39.

[22] A. Arora, J. Qin, D. C. Morse, K. T. Delaney, G. H. Fredrickson, F. S. Bates, K. D. Dorfman, Broadly accessible self-consistent field theory for block polymer materials discovery, Macromolecules 49 (13) (2016) 4675–4690.

[23] P. Knychała, K. Timachova, M. Banaszak, N. P. Balsara, 50th anniversary perspective: Phase behavior of polymer solutions and blends, Macromolecules 50 (8) (2017) 3051–3065.

[24] A. Chremos, A. Nikoubashman, A. Z. Panagiotopoulos, Flory-Huggins parameter χ, from binary mixtures of Lennard-Jones particles to block copolymer melts, J. Chem. Phys. 140 (5) (2014) 054909.

[25] Q. P. Chen, J. D. Chu, R. F. DeJaco, T. P. Lodge, J. I. Siepmann, Molecular simulation of olefin oligomer blend phase behavior, Macromolecules 49 (10) (2016) 3975–3985.

[26] W. Zhang, E. D. Gomez, S. T. Milner, Predicting Flory-Huggins χ from simulations, Phys. Rev. Lett. 119 (1) (2017) 017801.

[27] J. N. Owens, I. S. Gancarz, J. T. Koberstein, T. P. Russell, Investigation of the microphase separation transition in low-molecular-weight diblock copolymers, Macromolecules 22 (8) (1989) 3380–3387.

[28] C. Lin, S. Jonnalagadda, P. Kesani, H. Dai, N. Balsara, Effect of molecular structure on the thermodynamics of block copolymer melts, Macromolecules 27 (26) (1994) 7769–7780.

[29] A. K. Khandpur, S. Foerster, F. S. Bates, I. W. Hamley, A. J. Ryan, W. Bras, K. Almdal, K. Mortensen, Polyisoprene-polystyrene diblock copolymer phase diagram near the order-disorder transition, Macromolecules 28 (26) (1995) 8796–8806.

[30] H. Frielinghaus, N. Hermsdorf, K. Almdal, K. Mortensen, L. Messé, L. Corvazier, J. Fairclough, A. Ryan, P. Olmsted, I. Hamley, Micro-vs. macro-phase separation in binary blends of poly (styrene)-poly (isoprene) and poly (isoprene)-poly (ethylene oxide) diblock copolymers, EPL (Europhysics Letters) 53 (5) (2001) 680–686.

[31] M. J. Bluemle, J. Zhang, T. P. Lodge, F. S. Bates, Inverted phases induced by chain architecture in ABAC tetrablock terpolymers, Macromolecules 43 (10) (2010) 4449–4452.

[32] J. Zhang, S. Sides, F. S. Bates, Ordering of sphere forming SISO tetrablock terpolymers on a simple hexagonal lattice, Macromolecules 45 (1) (2011) 256–265.

[33] J. Zhang, F. S. Bates, Dodecagonal quasicrystalline morphology in a poly (styrene-b-isoprene-b-styrene-b-ethylene oxide) tetrablock terpolymer, J. Am. Chem. Soc. 134 (18) (2012) 7636–7639.

[34] S. Chanpuriya, K. Kim, J. Zhang, S. Lee, A. Arora, K. D. Dorfman, K. T. Delaney, G. H. Fredrickson, F. S. Bates, Cornucopia of nanoscale ordered phases in sphere-forming tetrablock terpolymers, ACS Nano 10 (5) (2016) 4961–4972.

[35] H. Frielinghaus, N. Hermsdorf, R. Sigel, K. Almdal, K. Mortensen, I. Hamley, L. Messe, L. Corvazier, A. Ryan, D. van Dusschoten, Blends of AB/BC diblock copolymers with a large interaction parameter χ, Macromolecules 34 (14) (2001) 4907–4916.

[36] H. Frielinghaus, W. B. Pedersen, P. S. Larsen, K. Almdal, K. Mortensen, End effects in poly (styrene)/poly (ethylene oxide) copolymers, Macromolecules 34 (4) (2001) 1096–1104.

[37] L. Leibler, Theory of microphase separation in block copolymers, Macromolecules 13 (6) (1980) 1602–1617.

[38] J. Glaser, P. Medapuram, T. M. Beardsley, M. W. Matsen, D. C. Morse, Universality of block copolymer melts, Phys. Rev. Lett. 113 (6) (2014) 068302.

[39] P. Medapuram, J. Glaser, D. C. Morse, Universal phenomenology of symmetric diblock copolymers near the order–disorder transition, Macromolecules 48 (3) (2015) 819–839.

[40] P. Medapuram, Investigation of universal behavior in symmetric diblock copolymer melts, Ph.D. thesis, University of Minnesota (2015).

[41] J. Qin, P. Grzywacz, D. C. Morse, Renormalized one-loop theory of correlations in disordered diblock copolymers, J. Chem. Phys. 135 (8) (2011) 084902.

[42] W. W. Maurer, F. S. Bates, T. P. Lodge, K. Almdal, K. Mortensen, G. H. Fredrickson, Can a single function for χ account for block copolymer and homopolymer blend phase behavior?, J. Chem. Phys. 108 (7) (1998) 2989–3000.

[43] T. M. Gillard, P. Medapuram, D. C. Morse, F. S. Bates, Fluctuations, phase transitions, and latent heat in short diblock copolymers: comparison of experiment, simulation, and theory, Macromolecules 48 (8) (2015) 2801–2811.

[44] G. H. Fredrickson, E. Helfand, Fluctuation effects in the theory of microphase separation in block copolymers, J. Chem. Phys. 87 (1) (1987) 697–705.

[45] J. Qin, D. C. Morse, Fluctuations in symmetric diblock copolymers: Testing theories old and new, Phys. Rev. Lett. 108 (23) (2012) 238301.

[46] A. A. Teran, N. P. Balsara, Thermodynamics of block copolymers with and without salt, J. Phys. Chem. B 118 (1) (2013) 4–17.

[47] L. Fetters, D. Lohse, D. Richter, T. Witten, A. Zirkel, Connection between polymer molecular weight, density, chain dimensions, and melt viscoelastic properties, Macromolecules 27 (17) (1994) 4639–4647.

[48] A. Arora, D. C. Morse, F. S. Bates, K. D. Dorfman, Accelerating self-consistent field theory of block polymers in a variable unit cell, J. Chem. Phys. 146 (24) (2017) 244902.

[49] J. G. Sprio, J. Yang, J. X. Zhang, M. A. Winnik, Experimental and theoretical investigation of the lamellar structure of a styrene-butyl methacrylate diblock copolymer by fluorescence resonance energy transfer, small-angle X-ray scattering, and self-consistent-field simulations, Macromolecules 39 (20) (2006) 7055–7063.

[50] J. Vavasour, M. Whitmore, Self-consistent field theory of block copolymers with conformational asymmetry, Macromolecules 26 (25) (1993) 7070–7075.

[51] M. Matsen, F. Bates, et al., Conformationally asymmetric block copolymers, J. Polym. Sci. Part B: Polym. Phys. 35 (1997) 945–952.

[52] M. W. Schulze, R. M. Lewis III, J. H. Lettow, R. J. Hickey, T. M. Gillard, M. A. Hillmyer, F. S. Bates, Conformational asymmetry and quasicrystal approximants in linear diblock copolymers, Phys. Rev. Lett. 118 (20) (2017) 207801.

[53] M. Liu, W. Li, F. Qiu, A.-C. Shi, Stability of the Frank–Kasper σ-phase in BABC linear tetrablock terpolymers, Soft Matter 12 (30) (2016) 6412–6421.

[54] B. Vorselaars, P. Stasiak, M. W. Matsen, Field-theoretic simulation of block copolymers at experimentally relevant molecular weights, Macromolecules 48 (24) (2015) 9071–9080.

[55] K. T. Delaney, G. H. Fredrickson, Recent developments in fully fluctuating field-theoretic simulations of polymer melts and solutions, J. Phys. Chem. B 120 (31) (2016) 7615–7634.

[56] G. H. Fredrickson, A. J. Liu, F. S. Bates, Entropic corrections to the Flory-Huggins theory of polymer blends: Architectural and conformational effects, Macromolecules 27 (9) (1994) 2503–2511.

[57] J. Dudowicz, K. F. Freed, Effect of monomer structure and compressibility on the properties of multicomponent polymer blends and solutions: 1. lattice cluster theory of compressible systems, Macromolecules 24 (18) (1991) 5076–5095.

[58] K. G. Honnell, J. G. Curro, K. S. Schweizer, Local structure of semiflexible polymer melts, Macromolecules 23 (14) (1990) 3496–3505.

[59] I. C. Sanchez, R. H. Lacombe, An elementary molecular theory of classical fluids. Pure fluids, J. Phys. Chem. 80 (21) (1976) 2352–2362.

[60] P. J. Flory, Fifteenth spiers memorial lecture. Thermodynamics of polymer solutions, Discuss. Faraday Soc. 49 (1970) 7–29.

[61] M. R. Khadilkar, S. Paradiso, K. T. Delaney, G. H. Fredrickson, Inverse design of bulk morphologies in multiblock polymers using particle swarm optimization, Macromolecules 50 (17) (2017) 6702–6709.

[14] S. Sioula, N. Hadjichristidis, E. L. Thomas, Novel 2-dimensionally periodic non-constant mean curvature morphologies of 3-miktoarm star terpolymers of styrene, isoprene, and methyl methacrylate, Macromolecules 31 (16) (1998) 5272–5277.

[15] T. Gemma, A. Hatano, T. Dotera, Monte carlo simulations of the morphology of ABC star polymers using the diagonal bond method, Macromolecules 35 (8) (2002) 3225–3237.

[16] K. Yamauchi, K. Takahashi, H. Hasegawa, H. Iatrou, N. Hadjichristidis, T. Kaneko, Y. Nishikawa, H. Jinnai, T. Matsui, H. Nishioka, et al., Microdomain morphology in an ABC 3-miktoarm star terpolymer: A study by energy-filtering TEM and 3D electron tomography, Macromolecules 36 (19) (2003) 6962–6966.

[17] K. Hayashida, T. Dotera, A. Takano, Y. Matsushita, Polymeric quasicrystal: Mesoscopic quasicrystalline tiling in ABC star polymers, Phys. Rev. Lett. 98 (19) (2007) 195502.

[18] M. W. Matsen, M. Schick, Stable and unstable phases of a diblock copolymer melt, Phys. Rev. Lett. 72 (16) (1994) 2660–2663.

[19] F. Drolet, G. H. Fredrickson, Combinatorial screening of complex block copolymer assembly with self-consistent field theory, Phys. Rev. Lett. 83 (21) (1999) 4317–4320.

[20] M. W. Matsen, The standard Gaussian model for block copolymer melts, J. Phys.: Condens. Matter 14 (2) (2001) R21.

[21] G. H. Fredrickson, V. Ganesan, F. Drolet, Field-theoretic computer simulation methods for polymers and complex fluids, Macromolecules 35 (1) (2002) 16–39.

[22] A. Arora, J. Qin, D. C. Morse, K. T. Delaney, G. H. Fredrickson, F. S. Bates, K. D. Dorfman, Broadly accessible self-consistent field theory for block polymer materials discovery, Macromolecules 49 (13) (2016) 4675–4690.

[23] P. Knychała, K. Timachova, M. Banaszak, N. P. Balsara, 50th anniversary perspective: Phase behavior of polymer solutions and blends, Macromolecules 50 (8) (2017) 3051–3065.

Supplementary Material for "Predicting the Phase Behavior of ABAC Tetrablock Terpolymers: Sensitivity to Flory–Huggins Interaction Parameters"

Akash Arora[a], Naveen Pillai[a,b], Frank S. Bates[a], Kevin D. Dorfman[a,c]

[a]*Department of Chemical Engineering and Materials Science, University of Minnesota–Twin Cities, 421 Washington Ave SE, Minneapolis, MN 55455, USA*
[b]*Present address: Department of Nuclear Engineering, North Carolina State University, Campus Box 7909, Raleigh, NC 27695, USA*
[c]*Email: dorfman@umn.edu*

Contents

S1. Multiple Converged Solutions

This section provides details of the density profiles and the other associated properties of the multiple converged SCFT solutions at the same state point obtained using different guess structures. These converged structures have different free energies owing to significantly different particle shapes and segregation of PI and PS blocks within the matrix.

S1.1. BCC Phase

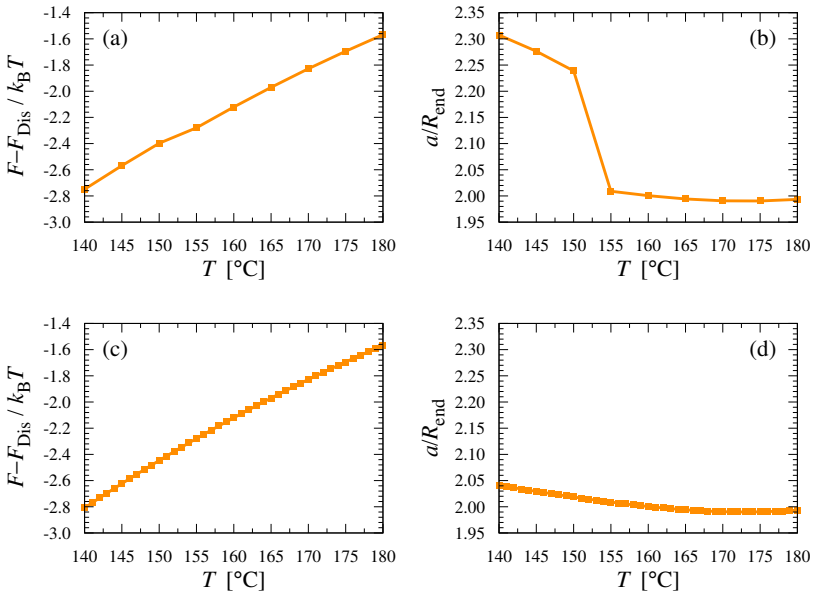

Figure S1: The relative free energy per chain, $F - F_{\mathrm{Dis}}/k_{\mathrm{B}}T$, and the unit-cell dimension of the BCC phase at $f_O = 0.13$ (SIS′O) for two sets of solutions obtained differently in the parameter space. The results in (a) and (b) are obtained using the converged solution at $(T, f_O + 0.01)$ as a guess structure to perform the SCFT calculation at (T, f_A). The results in (c) and (d) are obtained by supplying the converged solution of $(T + 1\ ^{\circ}\mathrm{C}, f_O)$ to perform the calculation at (T, f_O). These calculations are done using the interaction parameters of Approach 2.

Figure S1 shows the variation in free energy and unit-cell dimension of the BCC phase as a function of temperature. The results in Fig. S1 (a) and (b) correspond to the SCFT solutions obtained using the converged solution at $(T, f_O + 0.01)$ as a guess structure to perform the SCFT calculation at (T, f_A),

while Fig. S1c and d are obtained by supplying the converged solution of $(T + 1\ ^{\circ}\mathrm{C}, f_O)$ to perform calculation at (T, f_O). For $T \geq 155\ ^{\circ}\mathrm{C}$, both of the different procedures yield same results, however at $T = 155\ ^{\circ}\mathrm{C}$, the first procedure (Figs. S1a and b) experiences a discontinuity in unit-cell dimension, producing the significantly different structures shown in Fig. 5(a) in the main manuscript. Similar behavior is observed for the HCP phase, depicted in Fig. S2.

S1.2. HCP Phase

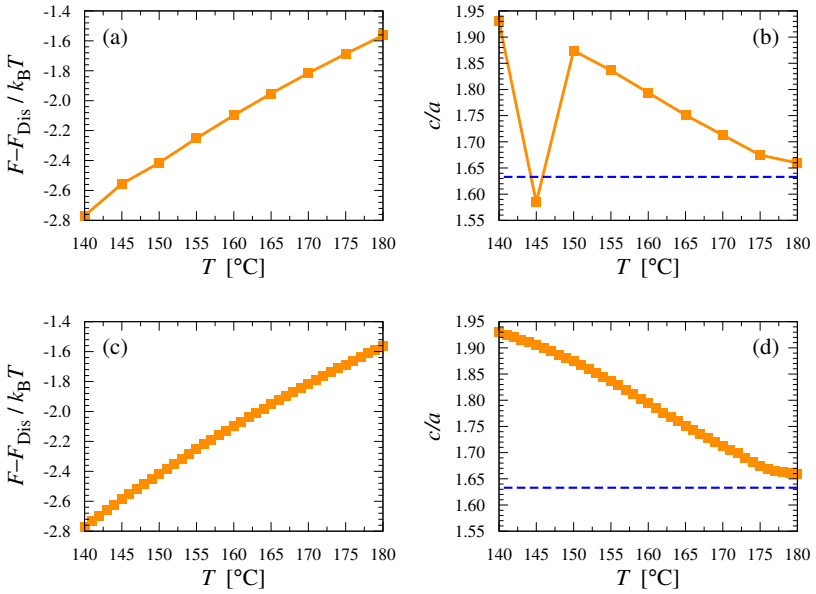

Figure S2: The relative free energy per chain $F - F_{\mathrm{Dis}}/k_{\mathrm{B}}T$, and the ratio of unit-cell dimensions, c/a, for the HCP phase at $f_O = 0.13$ (SIS′O) for two sets of solutions obtained differently in the parameter space. The solutions (a) and (b) are obtained using the converged solution at $(T, f_O + 0.01)$ as a guess structure to perform the SCFT calculation at (T, f_A). The solutions (c) and (d) are obtained by supplying the converged solution of $(T + 1\ ^{\circ}\mathrm{C}, f_O)$ to perform the calculation at (T, f_O). The dashed (blue) line in (b) and (d) denotes the ideal a/c ratio for the HCP structure, $a/c = 1.633$. These calculations are done using the interaction parameters of Approach 2.

S1.3. FCC Phase

Figures S3 and S4 show the density profiles of all the four blocks within the FCC phase for two converged solutions at $T = 140\ ^{\circ}\mathrm{C}$ and $f_{\mathrm{A}} = 0.13$

obtained using two different guess structures. The solution shown in Fig. S3 is obtained using the converged solution at ($T = 140$ °C, $f_A = 0.14$) as the guess structure, while the solution in Fig. S4 is obtained using the converged solution at ($T = 141$ °C, $f_A = 0.13$).

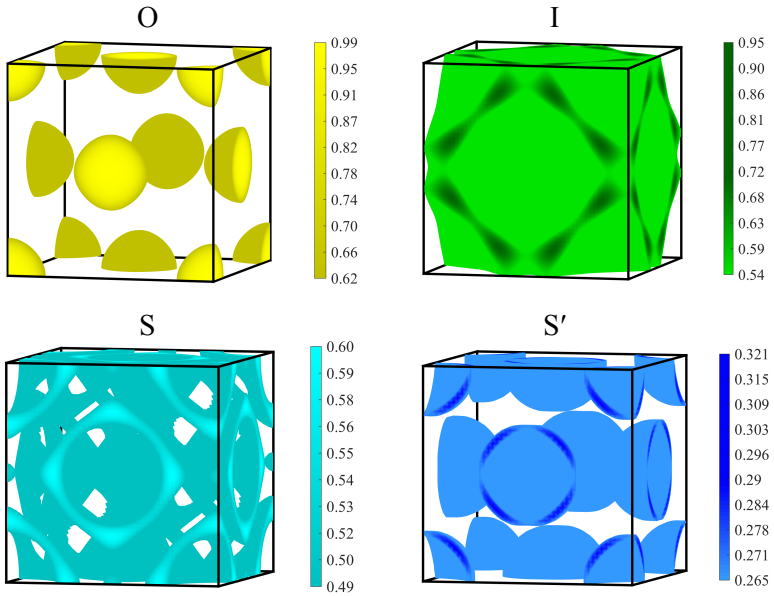

Figure S3: SCFT-computed density profiles of the FCC phase at $T = 140$ °C and $f_A = 0.13$. This calculation is done using the converged solution at ($T = 140$ °C, $f_A = 0.14$) as the guess structure and with Newton-Raphson iteration algorithm using the interaction parameters of Approach 2.

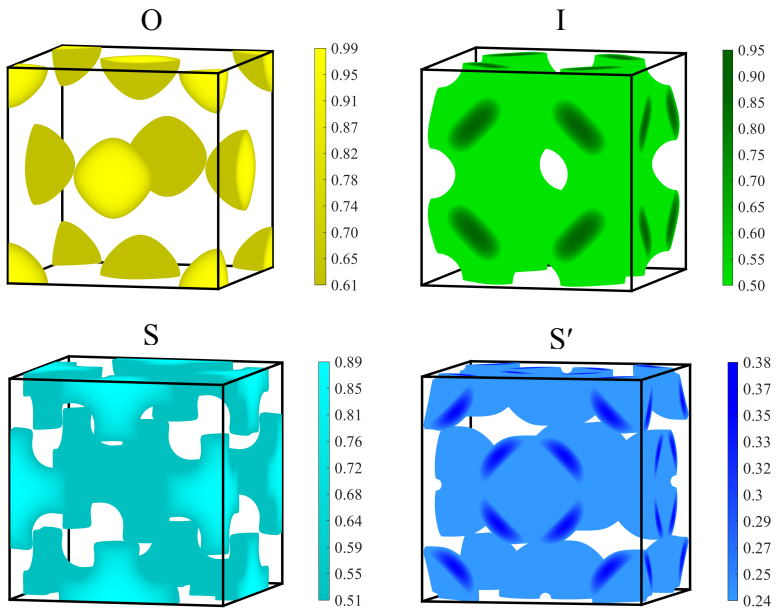

Figure S4: SCFT-computed density profiles of the FCC phase at $T = 140$ °C and $f_A = 0.13$. This calculation is done using the converged solution at ($T = 141$ °C, $f_A = 0.13$) as the guess structure and with Newton-Raphson iteration algorithm using the interaction parameters of Approach 2.

S2. Phase Transitions of Approach 2

Figure S5 shows the free energies of all of the six candidate structures relative to that of the BCC phase for the parameter space in the phase diagram of Approach 2 (Fig. 3b in the main manuscript) that exhibits extremely rich phase behavior.

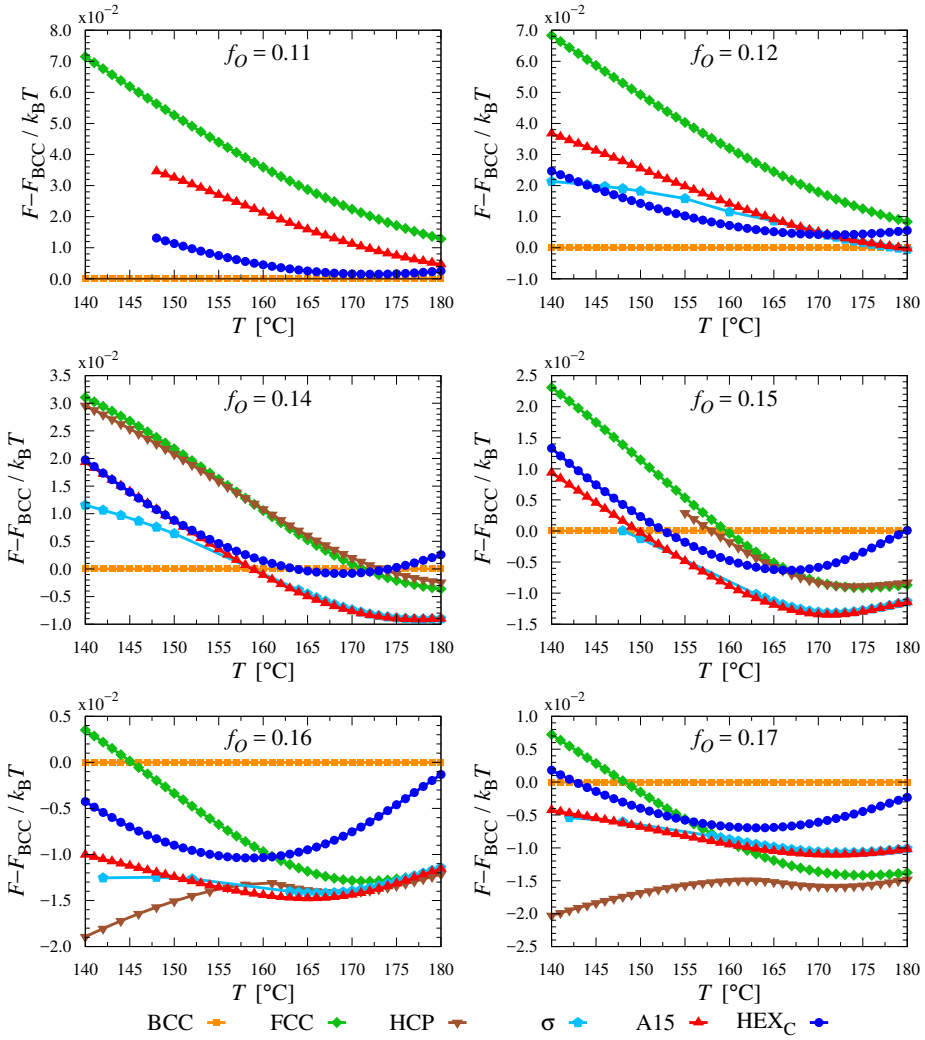

Figure S5: Relative free energies per chain, $F - F_{\mathrm{BCC}}/k_{\mathrm{B}}T$ for several different values of volume fraction, f_{O}, throughout the temperature range of the phase diagram of Approach 2 (Fig. 3b in the main manuscript).

S3. BCC-HEX$_C$ Boundary of Approach 3

Figure S6 shows the phase boundary between the BCC and HEX$_C$ phases in the phase diagram of Approach 3 (Fig. 3c in the main manuscript).

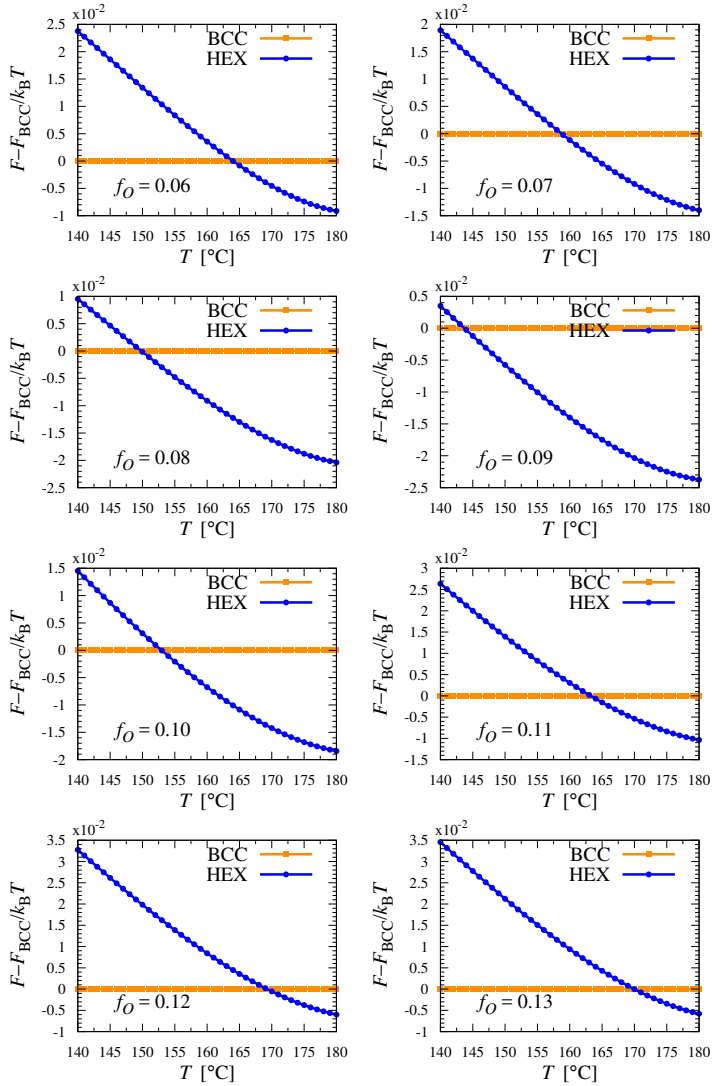

Figure S6: Relative free energies per chain, $F - F_{BCC}/k_BT$ of the BCC and HEX$_C$ phases for several different values of volume fraction, f_O, throughout the temperature range of the phase diagram of Approach 3 (Fig. 3c in the main manuscript).

S4. Uncertainties in SIS′O-0.73 Molecular Parameters

The SIS′0-0.73 polymer sample is synthesized using anionic polymerization method and the synthesis details are given in Ref. 40 of the main manuscript. The molecular parameters of the SIS′O-0.73 sample are determined by a combination of size-exclusion chromatography (SEC) and nuclear magnetic resonance (NMR) experiments. Specifically, the molecular weight of the first (terminal) PS block is measured by SEC using PS standards. Hence, the molecular weight of the terminal PS block is expected to be reasonably accurate. The number of repeat units of each subsequent block added is determined by ^{1}H NMR technique. In this procedure, the time-domain signal observed in ^{1}H NMR experiments is transformed into a frequency-domain signal and the area under the resulting peaks is computed to determine the number of repeat units, N. Once N_i for each block i is calculated, the corresponding molecular weights and volume fractions are calculated using the homopolymer melt densities. For SIS′O-0.73, the block molecular weights and volume fractions are calculated using the densities at $T = 140$ °C reported by Fetters *et al*. (Ref. 44 in the main manuscript). The overall uncertainty in the volume fraction is the convolution of the uncertainty arising from each ^{1}H NMR measurement (for SI, SIS′, and SIS′O) and the uncertainty in values of densities used. It is difficult to get a precise bound on the uncertainty, but based on the literature data, it is reasonable to expect a maximum uncertainty in volume fraction as $\Delta f_O = \pm 0.01$.

The polydispersity of SIS′O-0.73 is measured using SEC experiments using PS standards. The characterization of dispersity by SEC is based on the hydrodynamic volume of the polymer coils. Since the PS homopolymer and SIS′O tetrablock polymers of the same molecular weights may have different hydrodynamic volumes, the use of PS standards to calibrate and measure the dispersity is expected to introduce some amount of uncertainty in the reported value of Đ = 1.03. Assuming a Poisson distribution, the theoretical minimum value of polydispersity for SIS′O-0.73 having $M_n =$ 22.4 kDa ($N = 343$) is Đ =1.0029.